



# **JGR** Atmospheres

### **RESEARCH ARTICLE**

10.1029/2023JD040295

#### **Key Points:**

- Coherent coupling between cumulus and planetary boundary layer (PBL) parameterizations improves the nested rainfall diurnal cycle forecast
- Increasing cumulus parameterization frequency reduces the nested morning and outer-domain evening valley rainfall overforecast
- Adjusting PBL parameterization weakens the rainfall afternoon peak and daytime total amount overprediction

#### **Supporting Information:**

Supporting Information may be found in the online version of this article.

#### Correspondence to:

X.-Z. Liang and M. Zeng, xliang@umd.edu; swordzmj@qq.com

#### Citation:

Mei, H., Liang, X.-Z., Zeng, M., Yang, Y., Sun, C., & Li, X. (2024). Improving diurnal precipitation forecasts through coherent coupling of cumulus and planetary boundary layer parameterizations. *Journal of Geophysical Research: Atmospheres*, 129, e2023JD040295. https://doi.org/10.1029/ 2023JD040295

Received 1 NOV 2023 Accepted 16 MAY 2024

## Improving Diurnal Precipitation Forecasts Through Coherent Coupling of Cumulus and Planetary Boundary Layer Parameterizations

Haixia Mei<sup>1</sup>, Xin-Zhong Liang<sup>2,3</sup>, Mingjian Zeng<sup>1</sup>, Yang Yang<sup>4</sup>, Chao Sun<sup>2</sup>, and Xin Li<sup>1</sup>

<sup>1</sup>Key Laboratory of Transportation Meteorology of China Meteorological Administration, Nanjing Joint Institute for Atmospheric Sciences, Nanjing, China, <sup>2</sup>Earth System Science Interdisciplinary Center, University of Maryland, College Park, MD, USA, <sup>3</sup>Department of Atmospheric and Oceanic Science, University of Maryland, College Park, MD, USA, <sup>4</sup>Nanjing Vocational College of Information Technology, Nanjing, China

**Abstract** This study explores the impact of coupling cumulus and planetary boundary layer (PBL) parameterizations on diurnal precipitation forecasting during the plum rainy season in Jiangsu Province, China, using a double grid-nesting approach. Results show that coherent coupling of cumulus (only in the 15 km grid outer domain [O]) and PBL parameterizations leads to improved forecasting of diurnal variations in the morning, afternoon, and the evening. Increasing the frequency of the Kain-Fritsch (KF) cumulus scheme in [O] enhances subgrid precipitation while reducing grid-scale precipitation, resulting in a more accurate representation of daytime convective activities and a reduction in over-forecasting of evening valley and earlymorning precipitation. Additionally, coupling a suitable PBL scheme mitigates the overpredicted afternoon peak by facilitating turbulent mixing to penetrate higher altitudes with a thicker layer, thereby reducing instability energy accumulation. A higher KF frequency in [O] retains less low tropospheric moisture, reducing moisture convergence into the 1 km grid inner domain [I] and decreasing overpredicted daytime precipitation in [I]. Various PBL schemes produce distinct vertical distributions of turbulent moisture and heat transport, impacting convection and precipitation in [I] resolved by cloud microphysics processes. The coherent coupling of these parameterizations maintains a balanced supply of convective energy and water vapor, significantly improving diurnal precipitation forecasts in [I]. Isolating these parameterizations between nested grids may undermine this improvement.

Plain Language Summary Accurate diurnal precipitation forecasting remains a challenge. This study aims to effectively couple cumulus and planetary boundary layer (PBL) parameterizations to enhance diurnal precipitation forecasts using a double grid-nesting approach. We showed that coherent coupling of cumulus and PBL parameterizations improves forecasting of diurnal variations during the plum rainy season in Jiangsu Province, China. Increasing the frequency of the KF cumulus scheme more accurately represents daytime convective activities and reduces over-forecasting of evening valley and early-morning precipitation. Coupling an appropriate PBL scheme that extends turbulent mixing into deeper layers mitigates the accumulation of instability energy, thereby reducing overpredicting of the afternoon peak. A higher KF frequency in the 15 km grid outer domain [O] retains less low tropospheric moisture, reducing moisture convergence into the 1 km grid inner domain [I] and decreasing overpredicted daytime precipitation in [I]. Diverse PBL schemes result in varying vertical distributions of turbulent moisture and heat transport, affecting explicit convection and precipitation in [I]. Therefore, the cohesive integration of cumulus and PBL parameterizations across nested grids significantly enhances diurnal precipitation forecasts.

#### 1. Introduction

The ability to realistically predict the diurnal variation of precipitation is widely considered as an essential requirement for the model performance (Jin et al., 2016). Accurate reproduction of this variation has become a critical task for model improvement to enhance weather forecast and climate prediction capabilities. However, most models at relatively coarse grids that require cumulus parameterization (CUP) continue have difficulties to capture the diurnal variation at regional-local scales (Liang et al., 2004, 2019; Tang et al., 2021). Most simulations overestimate the diurnal cycle amplitude over land and produce the peak too early (Mooney et al., 2017). It remains challenging to understand the underlying physical processes and develop effective numerical solutions for the model deficiencies.

© 2024. American Geophysical Union. All Rights Reserved.

MEI ET AL.

Precipitation diurnal variation has strong regional dependence due to the combined effects of varying weather systems and complex surface characteristics. As the hinterland of economically developed and densely populated regions in China, Jiangsu Province is one of the major precipitation centers during summer as governed by the East Asian monsoon. It is adjacent to the East China Sea and has a generally flat topography with numerous low mountains, hills, and lakes. The summer rainfall diurnal variation in this region is characterized by two peaks, in the early morning and late afternoon, with a comparable intensity (Yu et al., 2007). The afternoon peak is mainly associated with convective precipitation induced by local thermal instability due to solar radiation heating (Xu & Zipser, 2011; Yu et al., 2007). The early morning peak is more complex as a result of interactions among the governing large-scale circulation, mesoscale convection, and multiscale topographic effects. General circulation models produce an earlier and more intensive afternoon peak (Yuan et al., 2013), and regional weather models also overestimate the afternoon peak intensity (Xue et al., 2018; Zhu et al., 2018).

CUP schemes are often considered to be the largest source of uncertainty in simulating diurnal precipitation variations (Konduru & Takahashi, 2020; Liang et al., 2004; Mooney et al., 2017; Qiao & Liang, 2015; Yuan et al., 2013). In coarse grid models that cannot explicitly resolve convection, CUP plays a critical role in capturing subgrid precipitation (Liang et al., 2019) and different schemes have significant impacts on the amplitude and phase of the diurnal cycle (He et al., 2015; Liang et al., 2004; Mooney et al., 2017; Pei et al., 2014; Qiao & Liang, 2015; Sun & Liang, 2023). Modifying CUP's trigger function can improve the diurnal phase (Jin et al., 2016) and suppress daytime convective activity (Qiao & Liang, 2015). Adjusting CUP's acting time scale can control the convection growth rate, affecting the diurnal variation or total precipitation amount (Gustafson et al., 2014). Changing CUP's entrainment rate can also affect the convection diurnal variation (Del Genio & Wu, 2010), for instance, enhancing the entrainment to detrainment ratio can delay the rainfall peak (Wang et al., 2007). Furthermore, altering CUP's closure assumption can regulate the diurnal phase and nighttime peak and greatly affect rainfall geographic distribution, frequency, and intensity (Bechtold et al., 2014; Liang et al., 2004, 2019; Qiao & Liang, 2016; Sun & Liang, 2023; Wong et al., 2020; Yang et al., 2018).

Many studies have shown that planetary boundary layer (PBL) parameterization also significantly affects the precipitation diurnal cycle. The afternoon peak over land is sensitive to PBL schemes in East Asia and across the southeastern and Gulf coastal United States (Koo & Hong, 2010; Mooney et al., 2017). PBL parameterization can cause excessive nighttime rainfall (Zhang & Chen, 2016) and affect the diurnal phase (He et al., 2015). It transfers surface turbulent fluxes of heat and moisture upward into the lower troposphere, which directly affects the accumulation of convective available potential energy (CAPE) and ultimately contributes to convective precipitation formation (Yang et al., 2018). It also transfers surface turbulent momentum flux upward to change winds in the boundary layer, alter the location and intensity of low-level jet and convergence zones, and thus indirectly affect the water vapor convergence (He et al., 2017). The latter ultimately changes the timing of rainfall onset, the distribution of rain areas, and the location and intensity of precipitation centers (Cai et al., 2006; Shen et al., 2017; Xu et al., 2013).

Diurnal precipitation variation can be significantly improved by models that explicitly resolve convection over those using CUP (Liang et al., 2019; Zhang et al., 2016). Due to the limitation of computational resources, operational forecasting is practically performed through grid nesting from an outer domain [O] using CUP with horizontal spacing around a few tens of kilometers to an inner domain [I] explicitly resolving convection at a few km spacing. Since [O] controls the simulation of the environment circulation, including synoptic-mesoscale advections and vertical motions, the result in [I] will be affected by the CUP scheme used in [O] (Liang et al., 2019; Warner & Hsu, 2000). Thus, CUP indirectly influences the diurnal characteristics of precipitation in [I]. In contrast, PBL parameterization is called in both [O] and [I] and typically with the same scheme for consistency. As such, different PBL schemes can interact with the CUP scheme in [O] to also affect the diurnal cycle of rainfall in [I] (Wang et al., 2021).

While PBL parameterization acts to generate/accumulate CAPE from surface forcing, CUP acts to consume/release CAPE through convective precipitation. Together, they form a loop influencing each other to regulate surface-atmosphere interaction and determine final precipitation. Their coupling effects can propagate across the nesting domains. Therefore, a joint test based on coupling cumulus and PBL parameterizations is more effective to address their sensitivities in simulating precipitation diurnal cycle. Studies on this topic are rare.

This study evaluates the individual and combined impacts of cumulus and PBL parameterizations on operational numerical weather prediction, using precipitation forecast in Jiangsu Province of China as a demonstration. It

MEI ET AL. 2 of 18

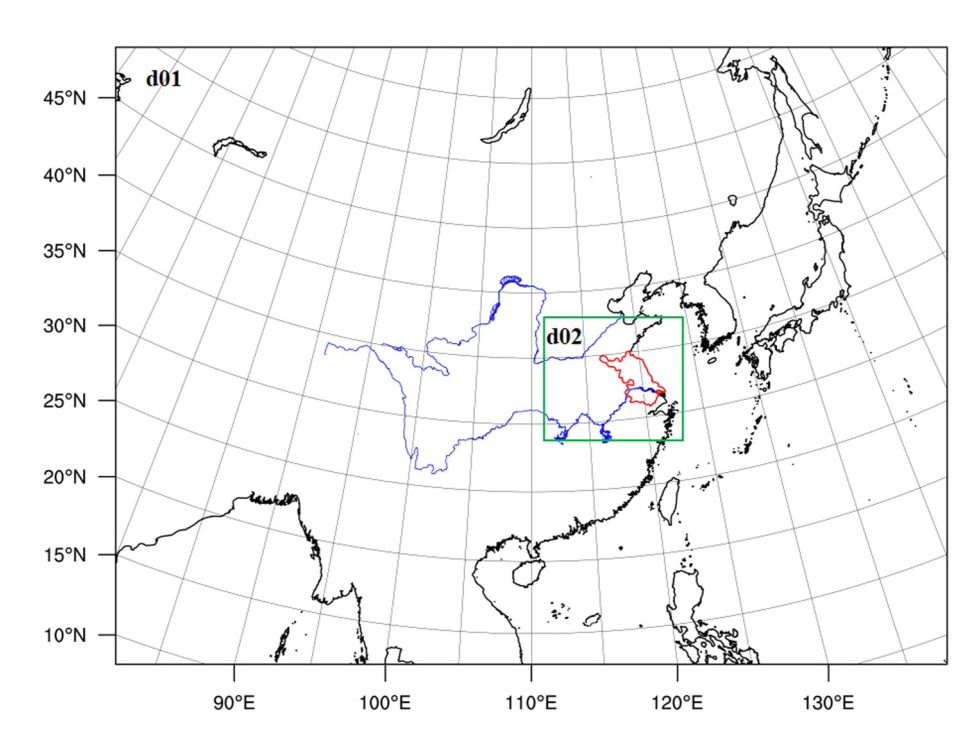


**Figure 1.** Model domain configuration with double nesting grids used in the forecast experiments, where the black (green) solid outline bounds the outer (inner) domain with grid spacing of 15 (a) km and red solid outline bounds the Jiangsu Province.

focuses on forecasting precipitation diurnal variation in a select month-long period of representative weather systems governing various convections over the region and examines the sensitivity to different CUP calling frequencies and PBL parameterization schemes. It addresses the ability of the coupling between cumulus (only in [O]) and PBL parameterizations to represent the diurnal cycle at different stages and determines the most coherent coupling configuration in the presence of the double nesting domains. The evaluation is concentrated on how they act jointly to improve forecasting the rainfall diurnal cycle in [I] and how their isolation affects the forcing-response processes across the nested grids.

#### 2. Methodology

## 2.1. Domain Configuration and Evaluation Period

The Weather Research and Forecasting (WRF) v3.9.1 model (Skamarock et al., 2008) is applied for the forecast experiments in this study. Figure 1 shows the computational domains and nesting grid configuration. Through systematic testing of various nests and resolutions, Liang et al. (2019) found that using 15 km grid spacing in [O] best captured regional precipitation distributions, and the nesting grid ratio of 15:1 configuration is most costeffective to realistically simulate [I] rainfall characteristics, including diurnal variations. Therefore, this double nesting approach is adopted in this paper. Specifically, the horizontal spacing of [O] is 15 km, with 463 west-east grids times 342 south-north grids, while the horizontal spacing of [I] is 1 km, with 1,156 times 1,021 grids. The lateral boundary conditions for [O] are updated at every 6-hr interval using the Global Forecast System (GFS) analysis at 0.5° (~55 km) grid spacing from the U.S. National Centers for Environmental Prediction (NCEP). We choose a one-way nesting strategy following the operational forecast procedure (i.e., no [I] feedback to [O]), and the integration time step is set to 6 s times the grid spacing in km for both domains.

The plum rainy season represents the seasonal northward progression of the East Asian Monsoon (Ding, 1992). It typically occurs from mid-June to mid-July (Tao & Chen, 1987) with a quasi-stationary west-east oriented rainband over the Yangtze-Huaihe River Basin of China, including Jiangsu Province (Samel et al., 1999). The rainy season is a common concern due to its characteristics of long duration, wide coverage, and frequent occurrence of heavy rainfall and convection. We choose the period from 19 June to 20 July in 2016 for a total of 32 days as the forecast skill evaluation. The total precipitation amount during this period in Jiangsu Province was

MEI ET AL. 3 of 18

double the climatological average, with a higher frequency of rainy events and a larger intensity range. It received much attention because of its catastrophic weather characteristics such as long impact time, frequent heavy rainfall, and outstanding extremes. The model is re-initialized at 12 UTC per day and integrated for 36-hr forecasts during the evaluation period. By employing the latest GFS analysis with improved accuracy as the initial state and lateral boundary conditions, this widely used approach (Goines & Kennedy, 2018; Xue et al., 2018; Yang et al., 2018) minimizes large-scale circulation forcing biases and hence is beneficial to prevent excessive growth of mesoscale forecast errors. It can not only reduce the synoptic forcing differences among the forecast sensitivity experiments, but also retain the sub-daily local-mesoscale processes to better capture the model ability in predicting diurnal variation. The initial period of less than 6 hr is considered as the spin-up, after which rainfall forecast characteristics are stable (Liang et al., 2019). The forecast skills are evaluated for the statistics calculated only in Jiangsu Province, comparing both [O] and [I] model results against observations. The area-averaged diurnal variations are obtained by the composite mean from 32 daily forecasts of 36 hr, including the first-day (0–24 hr) and the second-day (24–36 hr) after the start at 12UTC.

The rainfall data are provided by hourly accumulation measurements at the national assessment stations. These stations boast robust equipment maintenance, ensuring high stability, consistent data continuity, and utmost authenticity. Additionally, comprehensive quality control procedures are implemented, encompassing accuracy verification, temporal and spatial consistency check, as well as manual confirmation and correction of abnormal values. Following Liang et al. (2019), 1,238 stations with no missing records during the entire forecast period are selected over Jiangsu Province. The spacing among stations in the rain gauge network is approximately 9 km, which may be insufficient to capture complete rainfall characteristics, especially for evaluating extreme events in the fine grid. Furthermore, the European Center for Medium-Range Weather Forecasts 5th generation global reanalysis (ERA5, Hersbach et al., 2020) are used to cross-evaluate precipitation-relevant variables in absence of direct observations, including CAPE, water vapor supply, and surface latent and heat fluxes. The hourly ERA5 analysis was used to evaluate the coarse-grid forecasts only, as its resolution of 0.25° (~28 km) and use of CUP is not consistent with the fine-grid (1 km) explicitly resolving convection.

#### 2.2. Physics Parameterization and Experiment Design

The representative schemes of physical processes are kept consistent between the nested domains except that CUP is not used in [I]. The common parameterization schemes adopted from the operational forecast include Rapid Radiative Transfer Model longwave (Mlawer et al., 1997) and Goddard shortwave (Chou & Suarez, 1999) radiation, Thompson microphysics (Thompson et al., 2008), Kain-Fritsch (KF) cumulus (Kain, 2004), and unified Noah land surface (Tewari et al., 2004). This study explores the sensitivity of forecast skills for precipitation diurnal variation to altering the frequency calling the KF cumulus scheme and the choice of the PBL parameterization scheme, as detailed below.

Jin et al. (2016) found that the KF scheme with an optional trigger function based on water vapor advection can mitigate excessive precipitation amount and frequency and delay the diurnal afternoon peak over East Asia. On the other hand, Liang et al. (2019) concluded that two cumulus schemes with scale-aware algorithms (Grell & Freitas, 2014; Zheng et al., 2016, which is based on KF) may improve average precipitation performance in [O] but with larger counter errors to degrade overall forecast skills in double nesting [I]. Therefore, the traditional KF scheme (Kain, 2004) is chosen in this paper to facilitate the sensitivity analysis on its calling frequency.

Four PBL parameterization schemes commonly used in weather forecasts are selected for this sensitivity study. The control experiment uses the MYJ (Mellor-Yamada-Janjić) scheme (Janjić, 1994) as in the operational forecast. The other three are the YSU (Yonsei University, Hong et al., 2006), ACM (Asymmetric Convective Model version2, Pleim, 2007), and UW (University of Washington, Bretherton & Park, 2009) schemes. Both MYJ and UW are 1.5 order turbulence closure schemes that predict turbulent kinetic energy, while YSU and ACM are nonlocal mixing schemes that use the *K*-profile model of eddy diffusivity and viscosity. The surface layer parameterization is based on the Monin–Obukhov similarity, using the Eta algorithm (Janjić, 1996) to match with MYJ and the revised MM5 method (Jiménez et al., 2012) with other three PBL schemes.

Table 1 lists four groups of forecast experiments, examining effects of varying physics representations on rainfall diurnal variations in the coarse grid [O] by the first and second groups and in the fine [I] grid by the third and fourth groups. All groups contain a control experiment that calls KF cumulus scheme every 30 min or adopts MYJ PBL scheme as in the operational forecast. The first group tests the sensitivity of diurnal rainfall forecasts to the

MEI ET AL. 4 of 18

**Table 1**Summary of the Weather Research and Forecasting Model Nested Forecast Experiment Configurations

Outer domain [O] (grid spacing 15 km)					Inner domain [I] (grid spacing 1 km)		
		KF calling time interval [CT]					
Group	Experiment name	Frequency	Minute	PBL	Group	Experiment name	PBL
First	CT60	Low	60	MYJ	Third	CT60I	MYJ
	CT30 <sup>a</sup>		30			CT30I <sup>a</sup>	
	CT15	Medium	15			CT15I	
	CT6	High	6			CT6I	
	CT1.5		1.5			CT1.5I	
Second	$MYJ^{a}$	High	1.5	MYJ	Fourth	MYJI <sup>a</sup>	MYJ
	UW			UW		UWI	UW
	YSU			YSU		YSUI	YSU
	ACM			ACM		ACMI	ACM
Supplement	ACM/CT30	Low	30	ACM		ACMI/CT30	ACM
	UW_Eta	High	1.5	UW		UWI_Eta	UW

*Note.* MYJ and CT1.5 are a same test (so are MYJI and CT1.5I), using a different name only to depict their respective group of experiments. <sup>a</sup>The tests are regarded as the control forecast in each group. The lateral boundary conditions for the third (fourth) group are derived from the outputs of the first (second) group. The physics schemes in [I] are same as those in [O] except that KF cumulus is not used.

frequency calling KF in [O]. The call time interval (CT) in [minutes] is changed from 1.5 (equal to the dynamic integration step) and 6 for the high-frequency, 15 for the medium-frequency, and 30 (as the control) and 60 for the low-frequency; these experiments are abbreviated as CT1.5, CT6, CT15, CT30, and CT60 respectively. The CT6 is close to the CT5 used in Liang et al. (2019). Shorter CTs mean more frequent calls of CUP and hence more timely activation of the subgrid convection process when trigger conditions are met. Changes in CT can affect both cumulus feedback to large-scale thermodynamics and cloud microphysics, and thus alter the propagation, development, and precipitation of convective activities (Correia et al., 2008).

The second group tests the sensitivity of diurnal rainfall forecasts to the choice among the four PBL schemes in [O]. It uses the optimal KF call frequency (CT1.5) identified from the first group to minimize precipitation biases resulted from CUP and thus to better separate the effective influence of PBL parameterization. The outcome can help determine the best-combined effect of cumulus and PBL parameterizations in [O]. The third group tests the sensitivity of diurnal rainfall forecasts in [I] to different KF call frequencies in [O] and explores the underlying mechanisms. It uses the [O] outputs from the five CT experiments in the first group as the driving conditions to make the [I] forecasts. The fourth group tests the sensitivity of diurnal rainfall forecasts in [I] to different PBL schemes, each of which is identically adopted in the nested [O] and [I] grids. It uses the [O] outputs from the respective PBL experiments in the second group as the lateral boundary conditions driving the [I] forecasts. The outcome can reveal the role of the coherently coupled PBL and cumulus parameterizations across the nested grids.

Finally, a supplementary group tests the influence of switching the PBL scheme from MYJ to ACM as coupled with CT30 (vs. CT1.5) and matching the UW scheme with the same Eta surface layer algorithm as in the MYJ scheme. These two experiments are conducted in both [O] (ACM/CT30 and UW\_Eta) and [I] (ACMI/CT30 and UWI\_Eta) to examine the sensitivity of the PBL parameterization contribution to the coupling with different CTs and surface layer algorithms.

## 3. Sensitivity to Cumulus Parameterization Frequency in the Coarse Grid

## 3.1. Compensation Between Resolved and Parameterized Precipitation

Figure 2 compares observed and predicted diurnal variations of total precipitation averaged over all 32 daily forecasts in Jiangsu. Observations show two peaks in the early morning (08LT) and early afternoon (14LT)

MEI ET AL. 5 of 18

21698996, 2024, 11, Downloaded from https://aguputs.onlineltbrary.wiley.com/doi/10.1029/2023JD040295 by University Of Maryland, Wiley Online Library on [0807/2024]. See the Terms and Conditions (https://onlineltbrary.wiley.com/rems

-and-conditions) on Wiley Online Library for rules of use; OA articles are governed by the applicable Creativ

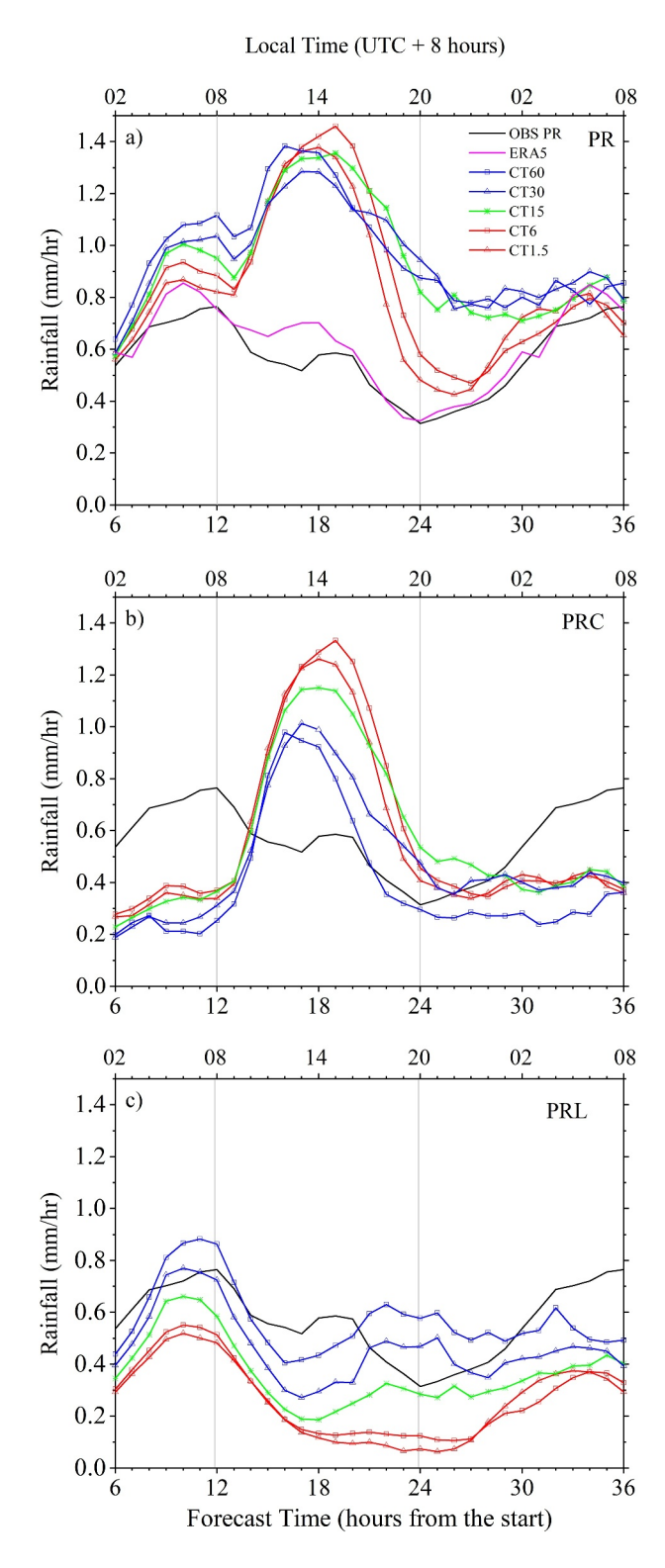
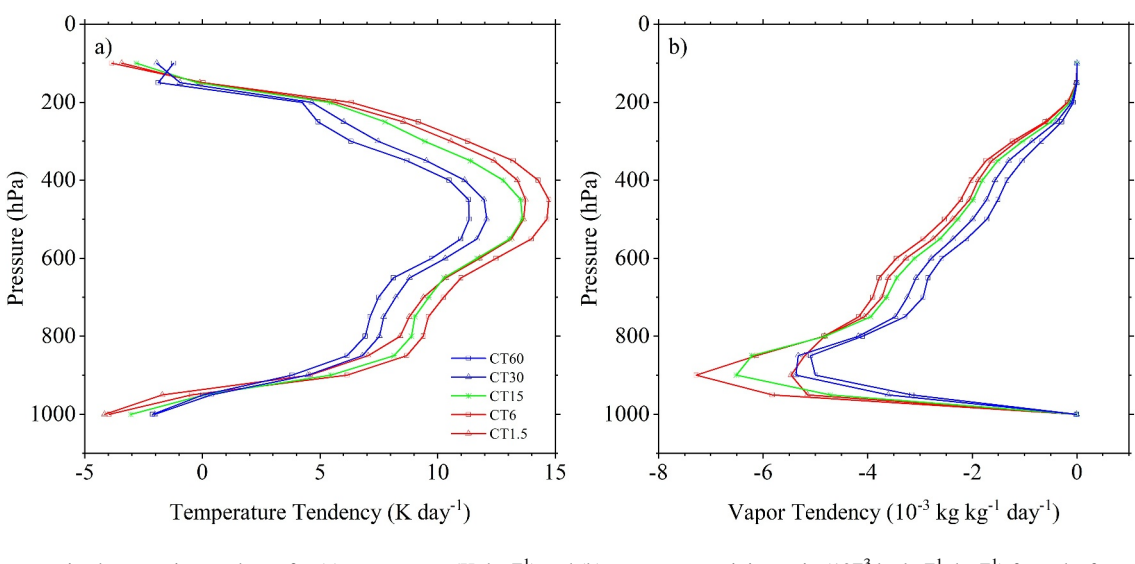


Figure 2. Area-averaged diurnal variation (mm/h) of (a) total precipitation (PR), (b) parameterized convective precipitation (PRC), and (c) resolved large-scale precipitation (PRL) from the forecasts in the coarse grid [O] for different Kain-Fritsch call frequencies (CTs) as compared with observations (OBS). The same observed total precipitation (OBS PR) is included in (b) and (c) to provide the diurnal cycle background information for easier interpretation of the resulting PRC and PRL responses. Included also in (a) is the total precipitation from ERA5 for comparison.

MEI ET AL. 6 of 18

21698996, 2024, 11, Downloaded from https://agupubs.onlinelibrary.wiley.com/doi/10.1029/2023JD040295 by University Of Maryland, Wiley Online Library on [08/07/2024]. See the Terms



**Figure 3.** The parameterized convection tendency for (a) temperature (K day<sup>-1</sup>) and (b) water vapor mixing ratio (10<sup>-3</sup> kg kg<sup>-1</sup> day<sup>-1</sup>) from the forecasts in the coarse grid [O] averaged in 11–16LT (local time), comparing different CTs.

and the valley in the evening (20LT). The control CT30 overestimates the precipitation intensity and shifts the diurnal phase: the first-day and second-day morning peaks being 35% and 20% higher, the afternoon peak more than doubled in magnitude and started earlier about 1 h, and the valley enhanced by 2.4 times and delayed about 2 h. Using CTs of 15- and 60-min leads to similar biases. Increasing the KF-call frequency improves the prediction. In particular, as compared to CT30, the high-frequency CUP (CT1.5, CT6) significantly reduces the overestimation of the first-day early morning (04-09LT) peak from 36% to 16%, 22% and the evening (19–01LT) valley from 140% to 35%, 49%. However, the substantial overestimation of the afternoon peak and overall daytime (11–18LT) precipitation remains or sometimes is even worsened. The ERA5-produced precipitation is generally close to observations, albeit with some overprediction during the

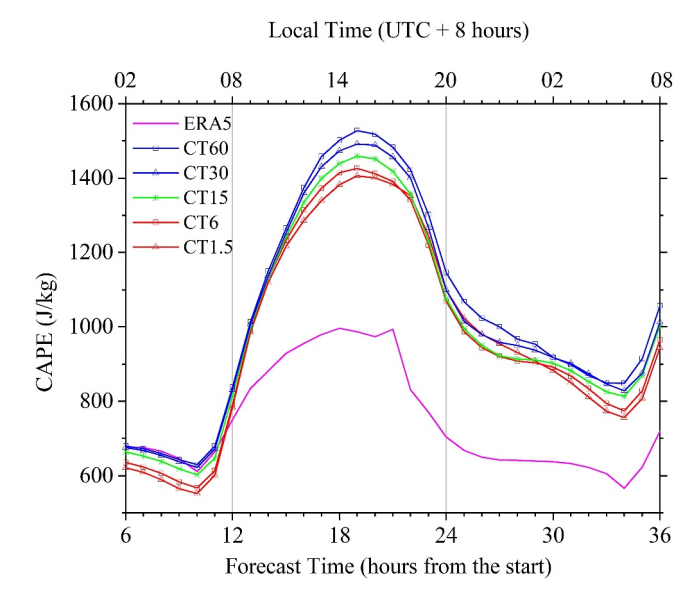


**Figure 4.** Area-averaged convective available potential energy (J/kg) diurnal variation from the forecasts in the coarse grid [O], comparing different CTs with ERA5 reanalysis.

early morning (05–07LT) and morning to afternoon (10–15LT) hours; this assessment is consistent with Jiao et al. (2021) and Zhou et al. (2023). Thus, the ERA5 analyzed environmental variables offer a good proxy of observations for cross-evaluation of the coarse-grid rainfall forecasts in Jiangsu Province. As compared to ERA5, the WRF overprediction of CAPE is improved during the daytime to nighttime hours by calling KF CUP more frequently. In particular, the CAPE's afternoon peak overestimation is reduced from 50% in CT30% to 41% in CT1.5 (Figure 4).

Total precipitation (PR) in [O] consists of parameterized convective precipitation (PRC) and resolved large-scale precipitation (PRL). As the frequency of CUP increases, PRC and PRL have important compensations, but their changes occur disproportionately. While PRL generally decreases, PRC has mixed changes in different times. During 04-10LT and 11-16LT, PRC increases. Increasing the frequency results in more cumulus convections, higher cloud tops, and deeper cloud systems throughout the day, and hence larger cloud droplet and ice crystal production rates. Consequently, the convective rainfall rate increases, while the convective warming and drying zone becomes thicker (Figure 3) and the overall CAPE weakens (Figure 4) due to respectively the enhanced latent heat release and instability energy depletion by timely triggering more convections. In 04–10LT, PRL decreases are larger than PRC increases, reducing the PR overestimation. In 11-16LT, opposite PRL and PRC changes compensate without causing a systematic PR trend, while the overestimation is sometimes enhanced as compared to the control run.

MEI ET AL. 7 of 18

During 17–02LT, PRC changes are mixed in sign and much smaller in magnitude than PRL decreases, leading to a significant reduction of the PR overestimation from using shorter CTs. Higher-frequency CUP does not bring more PRC around the evening due to the full consumption of CAPE by enhanced convections during the daytime. The more effective removal of available energy and water vapor weakens the environmental conditions for the development of the resolved precipitating cloud systems, the more slowly developing cloud microphysics processes produce substantially less precipitation, leading to disappearance of the PRL peak around 17–02LT, and thus significantly mitigate the overestimation of the PR valley.

Interestingly, increasing the CUP call frequency actually reduces the overall computational cost. On average, the total CPU time at a 55-teraflop computing power for a 36-hr forecast in [O] is 12, 9, 8.5, 8, and 8 min from CT60, CT30, CT15, CT6 to CT1.5, respectively. This reduction results mainly from the larger CPU saving in solving cloud microphysics than the additional cost for more frequent CUP. Timely triggering and full development of convections deplete more rainwater to eliminate grid-scale supersaturation conditions without the need for explicitly solving cloud microphysics.

#### 3.2. Weaker Afternoon Precipitation by High Frequent Cumulus Parameterization

Local convections are most active in the afternoon. In general, increasing the frequency of CUP from CT60, CT30, CT15 to CT6 enhances afternoon convective rainfall (Figure 2b). On the contrary, CT1.5 produces smaller PRC than CT6 during 13–18LT. In the morning to noon (08–13LT), CT1.5 generates more and earlier convective activities, with more frequent deep convections than CT6. In the afternoon (13–18LT), the convection development in CT1.5 is less sufficient, causing thinner clouds by 178 m on average and less drying but larger cooling below the cloud base (Figure 3a). The quicker CAPE consumption and more cloud raindrop evaporation lead to significantly weaker afternoon precipitation in CT1.5 than CT6.

The convective to total precipitation ratio is often inappropriately modeled (Tan et al., 2013; Wang et al., 2013). The high-frequency KF call in CT1.5 is conducive to the timely production of adequate PRC and the weakening of excessive PRL during the daytime, leading to a more appropriate partitioning between PRC and PRL. This benefits the improved prediction of total precipitation diurnal variation, for which the CT1.5 forecast is overall most realistic among all CTs. Therefore, CT1.5 (calling KF at each dynamic integration step) is considered as the optimal configuration for subsequent experiments.

#### 4. Sensitivity to PBL Parameterization in the Coarse Grid

## 4.1. Daytime Precipitation Reduction From Weaker CAPE Generation

Daytime precipitation is dominated by cumulus convections. The KF scheme consumes most of CAPE within a short time after convections are triggered (Fritsch & Kain, 1993). The optimal CUP configuration, CT1.5, still substantially overestimates the afternoon peak and overall daytime (10-16LT) precipitation, mainly due to overpredicting PRC (Figures 2a and 2b). The latter is driven by the significant overprediction of CAPE since the KF closure parameterizes convective precipitation directly with the CAPE release. On the other hand, the moisture supply overprediction contributes little to the PR overestimation during the afternoon peak hours. This results primarily from inadequate generation of grid-scale supersaturation conditions and phase changes to rain droplets and hence PRL, indicating the lack of suitable dynamic environment that enables precipitating cloud microphysics to develop. PBL parameterization transports turbulent heat and moisture fluxes upward as the main contributor to the CAPE generation (Yang et al., 2018). Thus, different PBL schemes can significantly affect the formation of convection and precipitation by altering the CAPE accumulation (Mooney et al., 2017). Figure 5 compares [O] precipitation forecasts among four PBL schemes as coupled with the KF cumulus CT1.5 configuration. Compared with the control MYJ, the other PBL schemes generally weaken the afternoon peak and daytime precipitation. Especially, ACM reduces the overprediction of the afternoon peak from 135% to 74%, rendering its rainfall forecast closest to observations. The daytime precipitation reduction results mainly from smaller PRC due to weaker CAPE produced by other PBL schemes (than MYJ). The CAPE generated from different PBL schemes can be consumed quickly by KF with high frequent cumulus convections and thus has little

The PBL turbulent transport produces significant heating and moistening mainly in the lower troposphere (Figure 6). During the daytime, the moistening penetrates higher and thicker layers using other PBL schemes than

MEI ET AL. 8 of 18

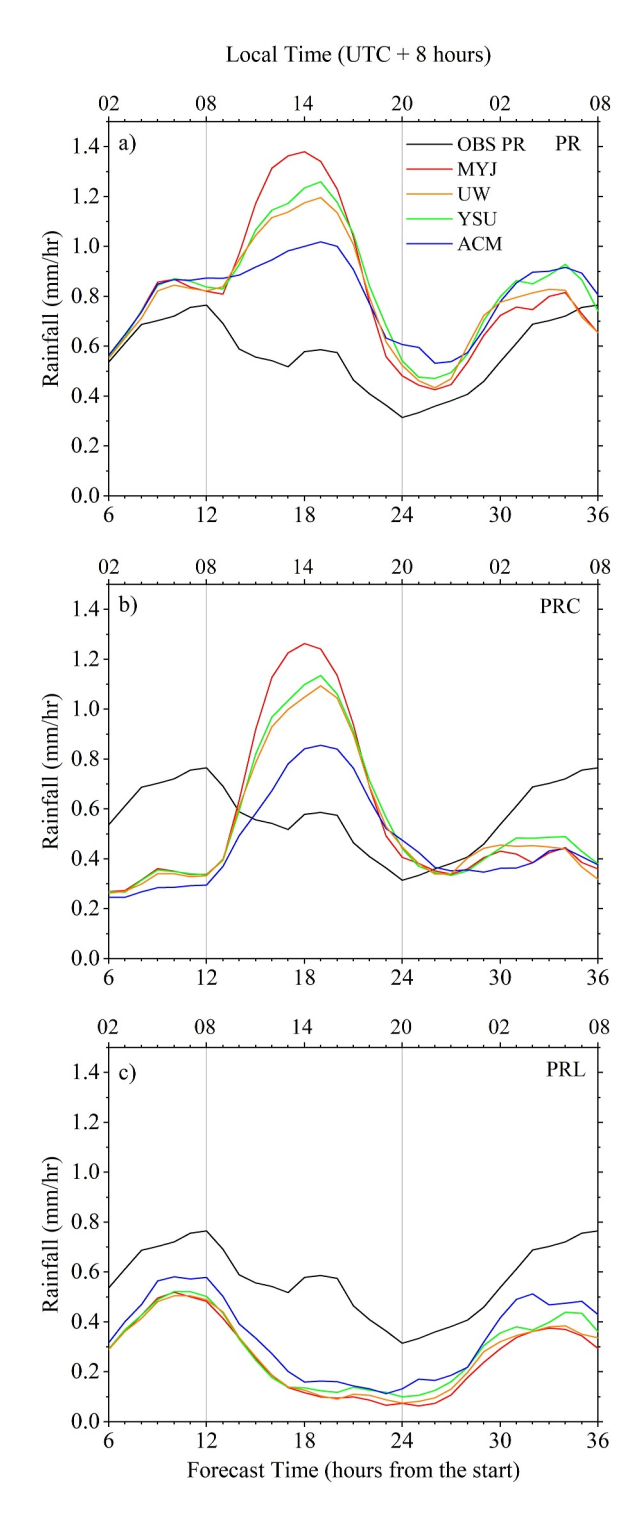


**Figure 5.** Same as Figure 2 except for comparing four planetary boundary layer parameterization schemes as coupled with CT1.5.

MYJ. This reduces the moistening peak significantly, for example, by 40% in ACM from MYJ. In addition, the temperature tendency exhibits a relatively shallow heating layer below 900 hPa, peaking near the surface layer around 1,000 hPa. As compared to MYJ, other schemes transport heat to somewhat higher layers and simulate larger cooling around 850 hPa.

The PBL turbulent mixing into deeper layers slows down the daytime CAPE generation, which in turn suppresses convection and precipitation. As a result, the overall convective heating and drying effects are weakened. Among the four PBL schemes tested, ACM produces the most significant reduction, with the peak convective heating and drying weakened by respectively 28% and 12% (Figure 7). Thus, using ACM allows slower CAPE generation, which favors convection to occur in later times and release the instability energy more gradually. This decreases rainfall around the afternoon peak but increases that in later hours.

The CAPE is considerably weakened, approaching closer to ERA5, during the daytime to nighttime hours by using other PBL schemes than MYJ. In particular, the peak overestimation is reduced from 41% in MYJ to 16% in YSU and 15% in UW, and even to become a 6% underprediction in ACM (Figure 8). The thicker moistening layer resulted from the PBL turbulent mixing leads to slower CAPE generation and weaker convection development and consequently lower precipitation. For example, UW and YSU have very similar PBL turbulent mixing tendencies and hence also generate almost same CAPE and convective precipitation. In contrast, ACM has the thickest moistening layer and consequently the weakest CAPE and lowest precipitation. The PBL mixing results in the accumulation of CAPE, which subsequently fuels the development of convection as it consumes the stored CAPE.

Recall that the experiments using the MYJ and other PBL schemes differ also in their matching surface layer parameterization, using the Eta (Janjić, 1996) versus revised MM5 (Jiménez et al., 2012) algorithms, which may cause surface forcing contrasts in addition to PBL turbulent mixing effects. Figure S1 in Supporting Information S1 compare precipitation partitions (PR, PRC, PRL), CAPE, and surface sensible and latent heat fluxes between UW and UW\_Eta that is coupled with the Eta instead of MM5 surface layer algorithm. While sensible heat flux differs little, latent heat flux during the daytime is systematically larger in UW\_Eta than UW by 14 [W m<sup>-2</sup>] (5%). Thus, UW\_Eta produces larger CAPE between 10 and 02LT by 56 [J kg<sup>-1</sup>] (6%), showing a sustained effect over a longer duration. The resulting total precipitation in the daytime between 09 and 16LT is slightly higher in UW\_Eta by 0.05 [mm/hr] (5%), due mostly to the convective rainfall enhancement. As compared to the spread among different PBL (mixing) schemes, these differences from surface layer parameterization are less significant.

# **4.2. Precipitation Regulation by Combined Cumulus and PBL Parameterizations**

Since PBL and cumulus parameterizations determine respectively CAPE's accumulation and consumption, their combined effects regulate precipitation formation and diurnal variation. As coupled with the MYJ PBL parameteri-

zation, the KF CUP called at a high frequency (CT1.5) ensures timely CAPE release and proper PRC and PRL partition, avoids daytime precipitation delay, and reduces early morning and nighttime low-rainfall over-prediction (Figure 2). The MYJ/CT1.5 coupling, however, still substantially overpredicts daytime precipitation. This daytime overprediction is significantly reduced by coupling the ACM PBL scheme with low frequent CUP (ACM/CT30), which results in an improved daytime precipitation peak but worsened nighttime low-rainfall

MEI ET AL. 9 of 18

21698996, 2024, 11, Downloaded from https://agupubs.onlinelibrary.wiley.com/doi/10.1029/2023JD040295 by University Of Maryland, Wiley Online Library on [08/07/2024]. See the "

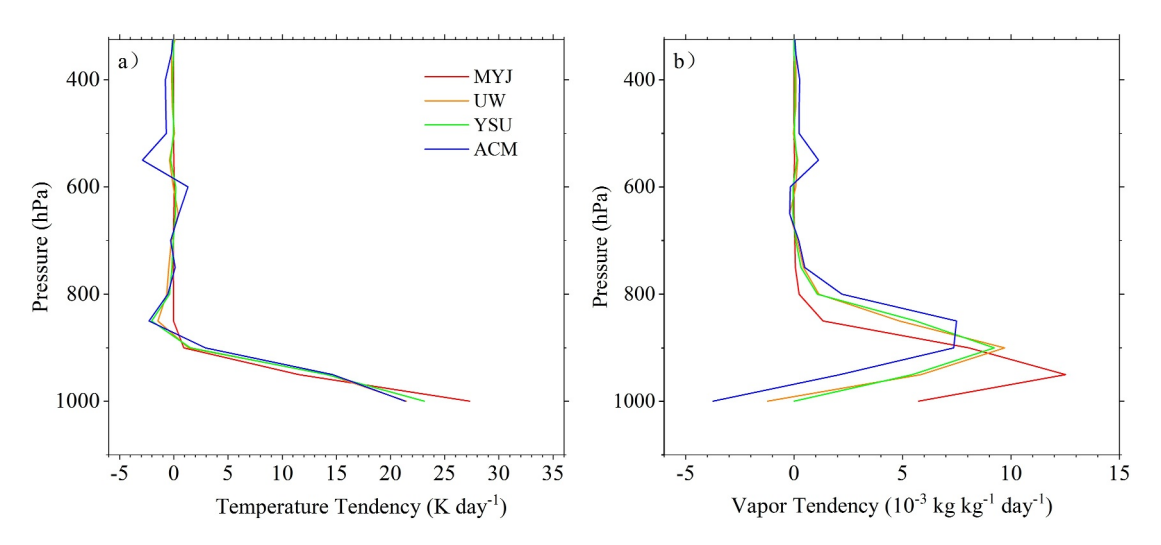


**Figure 6.** The parameterized planetary boundary layer (PBL) turbulence tendency for (a) temperature (K day<sup>-1</sup>) and (b) water vapor mixing ratio (10<sup>-3</sup> kg kg<sup>-1</sup> day<sup>-1</sup>) from the forecasts in the coarse grid [O] averaged in 11–16LT, comparing different PBL schemes.

overprediction with a false weak peak around the observed valley (Figure S1a in Supporting Information S1). The opposite daytime versus nighttime result occurs because PRL increases during the afternoon to evening hours as lagged compensation to reduced PRC from low frequent CUP.

When coupling with high frequent CUP (CT1.5), the ACM PBL parameterization based on the ACM replacing MYJ scheme significantly improves the precipitation diurnal variation forecast throughout the entire period. The ACM/CT1.5 coupling also avoids the false nighttime peak in ACM/CT30. These results demonstrate the critical role of coherent coupling between cumulus and PBL parameterizations on precipitation diurnal cycle forecast. There remains a large room for optimizing the coupling to improve the forecast of the daytime peak.

#### 5. Fine-Grid Forecast Sensitivity to Cumulus Parameterization Frequency

Different CUP schemes in the outer grid [O] have a significant effect on diurnal rainfall forecast in the inner grid [I] through the driving mesoscale circulation changes (Liang et al., 2019). Calling KF at a lower frequency results in overall higher rainfall (Figure 9), especially in the first day from the early morning to early afternoon (02–15LT). For example, CT60I, as compared to CT1.5I, alters the first-day morning peak from a 4% underprediction to a 9% overestimation and enhances the afternoon peak overprediction from 32% to 42%.

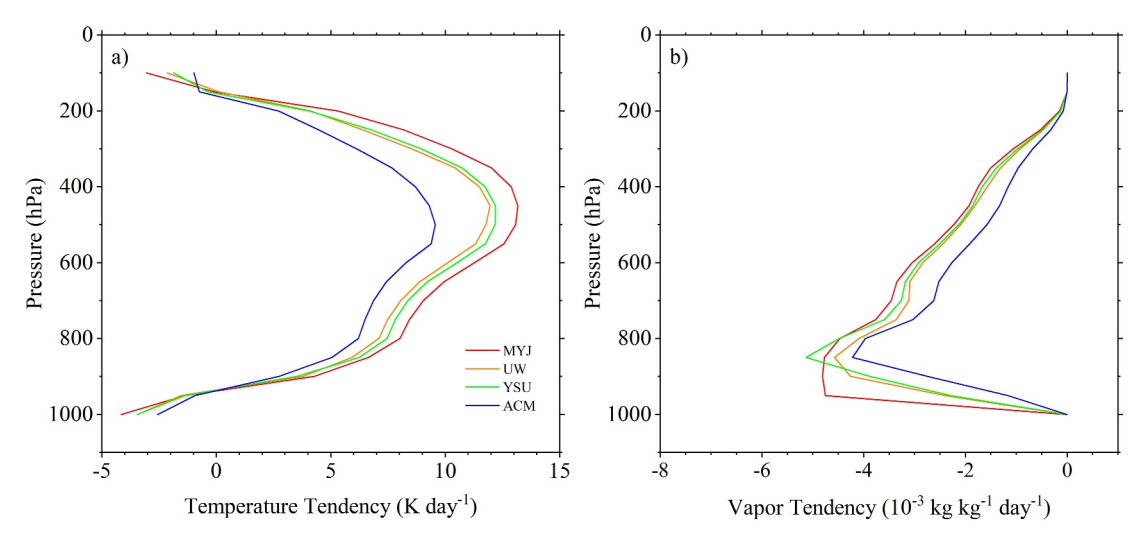
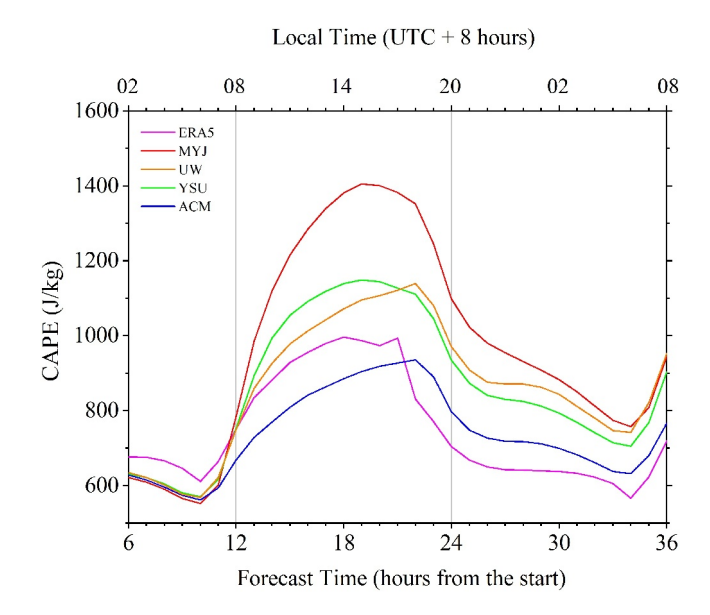


Figure 7. Same as Figure 3 except for comparing different planetary boundary layer schemes.

MEI ET AL. 10 of 18



**Figure 8.** Same as Figure 4 except for comparing different planetary boundary layer schemes.

The water vapor supply for precipitation consists of atmospheric moisture horizontal convergence and surface evapotranspiration (Figure 10). There is a net atmospheric inflow of water vapor to Jiangsu, with nighttime values ranging from 8.0 to 24.8 [mm day<sup>-1</sup>]. This inflow peaks at 04–05LT and gradually decreases during the daytime, reaching near-zero levels at 18LT. In contrast, surface evapotranspiration primarily contributes during the daytime, varying from 0.3 to 11.1 [mm day<sup>-1</sup>] and reaching its peak around noon at 13LT. Thus, moisture convergence outside Jiangsu dominates the nighttime to morning water vapor supply, with its maximum occurring approximately 2 hr before the early morning rainfall peak at 06–07LT. On the other hand, evapotranspiration becomes the major contributor from noon to early evening (12–18LT), with its maximum occurring approximately 2–3 hr before the afternoon rainfall peak at 14–16LT. Both sources contribute with a similar magnitude during the quick transition around 10–11LT.

Among the forecasts using the same MYJ PBL and surface layer parameterization schemes, evapotranspiration changes little under the same representation of surface-atmosphere interaction, while moisture convergence differences among varying cumulus treatments in [O] are significantly large (up to a 36 hr-mean of 2.6 kg m<sup>-2</sup> day<sup>-1</sup>). This indicates the dominant role of the coarse-grid forecasts, providing the mesoscale circulation to drive the development of the precipitation processes in the inner domain. Therefore, precipitation enhancement in the inner grid [I] from decreasing the frequency

calling KF in the outer grid [O] is primarily contributed to increases in moisture convergence rather than changes in evapotranspiration. CT60I, as compared to CT1.5I, increases moisture convergence by 9% and 45% during nighttime and afternoon peaks, respectively. Reducing frequency of KF calls leads to insufficient convective activity, causing the buildup of CAPE and the retention of moisture, particularly in the lower troposphere of [O]. The increased instability and moisture in [O] then propagate into [I], providing additional energy and water vapor for enhanced precipitation.

#### 

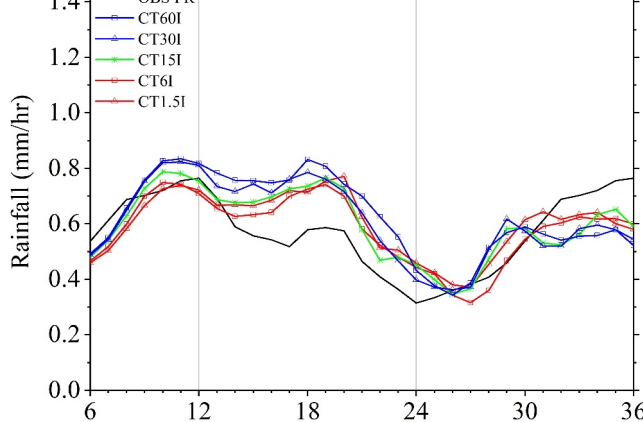


**Figure 9.** Area-averaged diurnal variation of total precipitation (mm/h) from the inner grid [I] forecasts at different frequencies calling Kain-Fritsch (CTs) in the outer grid [O] as compared with observations.

Forecast Time (hours from the start)

## 6. Fine-Grid Forecast Sensitivity to PBL Parameterization

### 6.1. Daytime Precipitation Link to Turbulent Mixing Transport

Recall that both the coarse outer [O] and fine inner [I] grids use a same PBL scheme. The control run using the MYJ scheme overall overestimates the daytime [I] precipitation, which is consistent with the result of Schwartz et al. (2010). The sensitivity runs using other PBL schemes generally reduce the over-forecast for the daytime (08–21LT) rainfall and its afternoon peak (Figure 11). UW, ACM, and YSU produces systematically weaker daytime precipitation than MYJ, reducing the overprediction of the afternoon peak from 32% to 11%, 16%, and 31%, respectively.

Such precipitation weakening is associated with changes in vertical moisture transport and CAPE generation due to PBL turbulent mixing differences. As compared to MYJ, UW, ACM, and YSU transport water vapor to higher layers (Figure 12), leaving less water in near-surface layers and thus discouraging CAPE accumulation (Figure 13a). YSU produces a deeper moistening layer extending up to 800 hPa, but its peak is about third from MYJ. ACM further elevates the moistening layer. In contrast, UW has a moistening layer similar to MYJ but with a peak reduced by 60% near the surface layer. Both ACM and UW have a secondary moistening layer between 700 and 400 hPa, peaking around 600 hPa. The ACM water vapor tendency shows negative values near the surface with a drying effect, which results from a stronger turbulent mixing along with transport to higher layers. A similar phenomenon is present in the coarse grid (Figure 6b) albeit less

MEI ET AL. 11 of 18

08

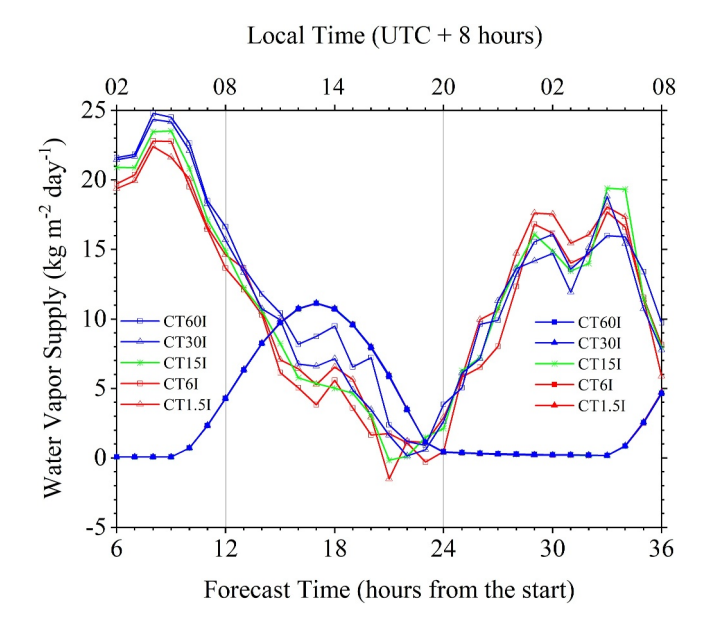


**Figure 10.** Same as Figure 9 except for water vapor supply terms (kg m<sup>-2</sup> day<sup>-1</sup>): atmospheric moisture net horizontal convergence (hollow markers) and surface evapotranspiration (solid markers).

pronounced. In addition, the result at 1,000 hPa may be discounted due to the average excluding some grids with lower surface pressures.

On the other hand, the temperature tendency due to PBL turbulent mixing produces a relatively shallow heating layer, peaking near the surface layer around 1,000 hPa. As compared to MYJ, YSU, and UW, ACM transports heat to somewhat higher layers and the heating peak intensity decrease from MYJ, UW, ACM to YSU, with a daytime (11–16LT) average from 35.3, 29.7, 29.2 to 26.3 (K day<sup>-1</sup>).

This trend is different to the decreasing trend in surface sensible heat flux (Figure 13b) from MYJ, YSU, UW to ACM, with a daytime average from 75.3, 72.3, 70.2 to 64.9 (W m<sup>-2</sup>). A similar decreasing trend occurs in surface latent heat flux, with a daytime average from 159.0, 150.2, 149.2 to 147.1 (W m<sup>-2</sup>). The CAPE diurnal variation and its decreasing trend from MYJ, YSU, UW to ACM follows closely with those of both surface fluxes, indicating the dominant role of PBL parameterization in providing surface sources for CAPE. However, total precipitation has a different trend, decreasing from MYJ, YSU, ACM to UW, with a daytime average from 0.61, 0.60, 0.57 to 0.53 (mm day<sup>-1</sup>). The result suggests that precipitation in the inner grid [I] explicitly resolved by cloud microphysics processes is disconnected from CAPE accumulation but driven more by vertical distributions of PBL turbulent moisture and heat transport.

Figure S2 in Supporting Information S1 compares precipitation partitions (PR, PRC, PRL) between UW and UW\_Eta that is coupled with the Eta instead of MM5 surface layer algorithm. The resulting absolute differences of

PR between UW and UW\_Eta in the daytime (09-16LT) are small, by 0.01 [mm/hr] (2%). This is similar to the result of the coarse gird that the differences from surface layer parameterization are less significant as compared to the spread among different PBL (mixing) schemes.

#### 02 08 02 08 OBS PR - MYJI -UWI YSU 1.2 ACMI Rainfall (mm/hr) 1.0 0.4 0.2 0.0 12 18 24 36

Local Time (UTC + 8 hours)

**Figure 11.** Same as Figure 9 except for comparing different planetary boundary layer schemes.

Forecast Time (hours from the start)

#### 6.2. Daytime Incoherence Between Precipitation and CAPE

Recall that there exists a strong correspondence during the daytime between differences in precipitation (Figure 2) and CAPE (Figure 4) among the forecasts in the coarse outer grid [O] from varying CUP frequencies (Figure 2 vs. Figure 4) or using different PBL schemes (Figure 5 vs. Figure 8). Such correspondence results from the KF closure that parameterizes convective precipitation directly with CAPE release. The correspondence is broke down among the forecasts in the fine inner grid [I] from different PBL schemes (Figure 11 vs. Figure 13a), where convection and precipitation are explicitly resolved as a coupled system by cloud microphysics processes. The characteristics of CAPE diurnal variation and its contrast among PBL schemes in [I] (Figure 13a) follow closely with those in [O] (Figure 8) except for a systematic reduction in magnitude. Thus, PBL parameterization remains the same source for CAPE generation: MYJ is the largest, ACM the lowest, while UW and YSU fall in the middle. The accumulated CAPE, however, is no longer consumed proportionally by precipitation in [I]. While MYJ still exhibits the highest values for both rainfall and CAPE, ACM shows greater rainfall but smaller CAPE compared to UW, thereby reversing the rainfall-CAPE correspondence.

On average, ACM exhibits a larger area with weaker intensity of upward motion and condensation compared to UW (Figure 14). This suggests that ACM's turbulent mixing is likely to drive more widespread and relatively weaker cloud systems, thereby depleting CAPE more promptly. Precipitation resulting from microphysical processes aims to eliminate grid-resolved

MEI ET AL. 12 of 18

21698996, 2024, 11, Downloaded from https://agupubs.onlinelibrary.wiley.com/doi/10.1029/2023JD040295 by University Of Maryland, Wiley Online Library on [08/07/2024]. See the "

of use; OA articles are governed by the applicable Creatir

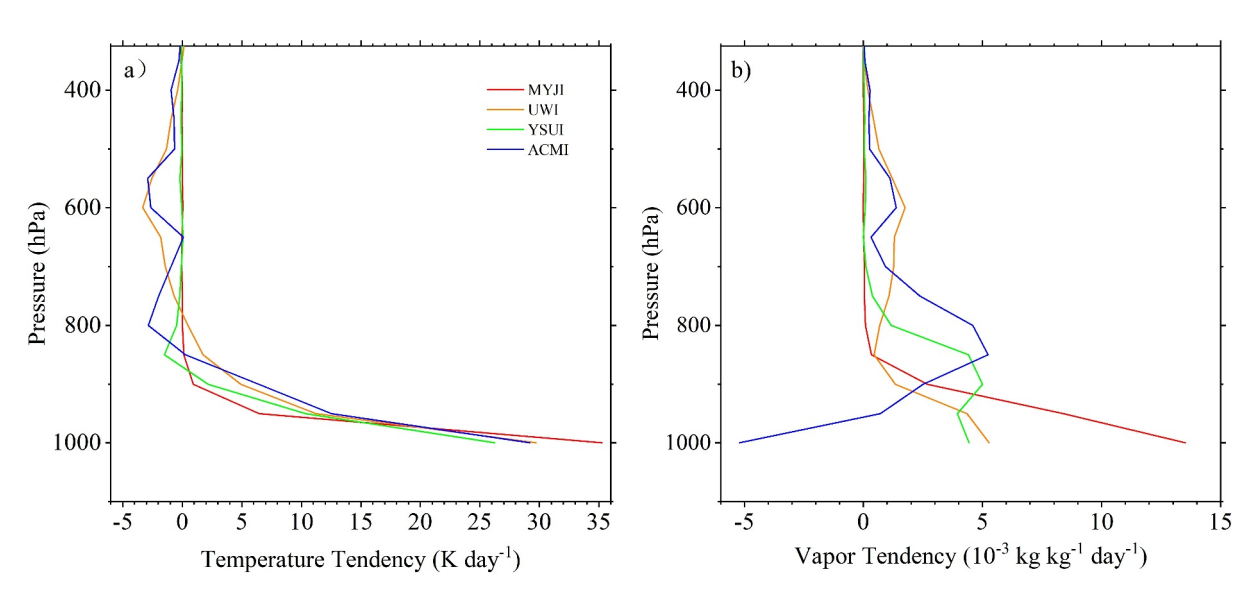


Figure 12. Same as Figure 6 except for the [I] forecasts.

supersaturation rather than depleting CAPE completely through CUP. Compared to UW, ACM produces higher rainfall through a stronger net production by phase change alongside a smaller atmospheric storage due to a sufficient conversion of cloud to rain droplets (Figure 15). As a result, the correspondence between rainfall and CAPE is much weaker in [I] when using explicit convection compared to [O] utilizing CUP.

#### 6.3. Coherent Coupling of Cumulus and PBL Parameterizations

The coarse outer grid [O] represents the synoptic and mesoscale circulation processes that provide the lateral boundary conditions driving the coupled and explicitly resolved convection and precipitation forecasts in the fine inner grid [I]. More frequent CUP in [O] releases CAPE more promptly through convective precipitation, depleting moisture from the atmosphere and reducing water vapor transport into [I]. Consequently, CT1.5 alleviates over-forecasting of precipitation in [I], particularly in the morning, although the daytime over-forecast remains substantial. Different schemes of PBL parameterization alter the vertical distributions of turbulent heat and moisture mixing as well as surface fluxes for CAPE accumulation,

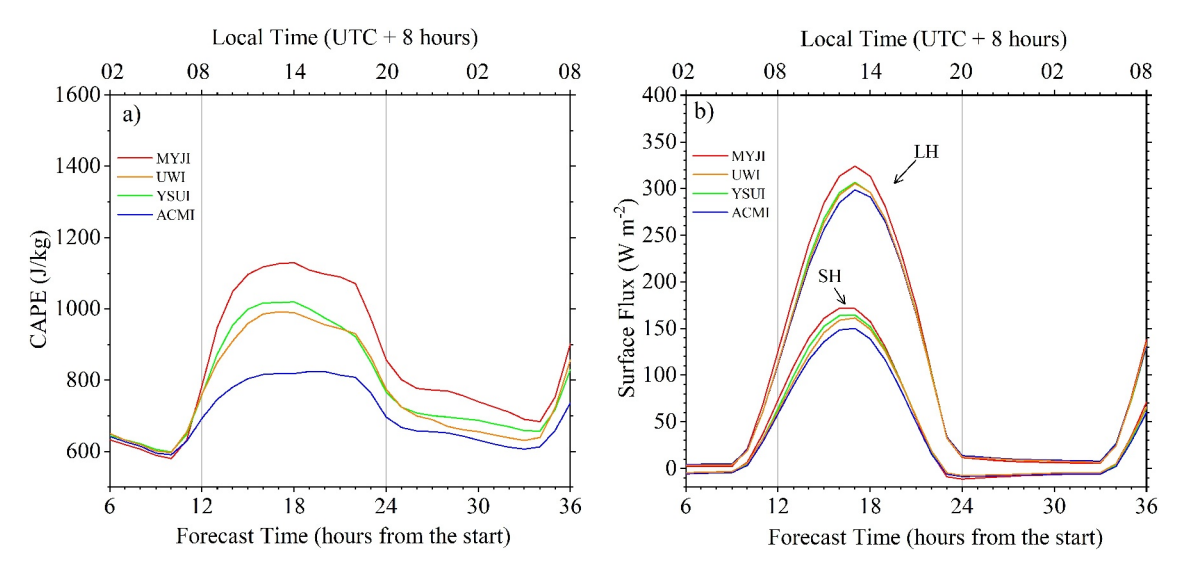


Figure 13. Area-averaged diurnal variations of (a) convective available potential energy (J/kg) and (b) surface latent (LH) and sensible (SH) heat fluxes (W m<sup>-2</sup>) from the forecasts in the fine grid [I], comparing different planetary boundary layer schemes.

MEI ET AL. 13 of 18

21698996, 2024, 11, Downloaded from https://agupubs.onlinelibrary.wiley.com/doi/10.1029/2023JD040295 by University Of Maryland, Wiley Online Library on [08/07/2024]. See

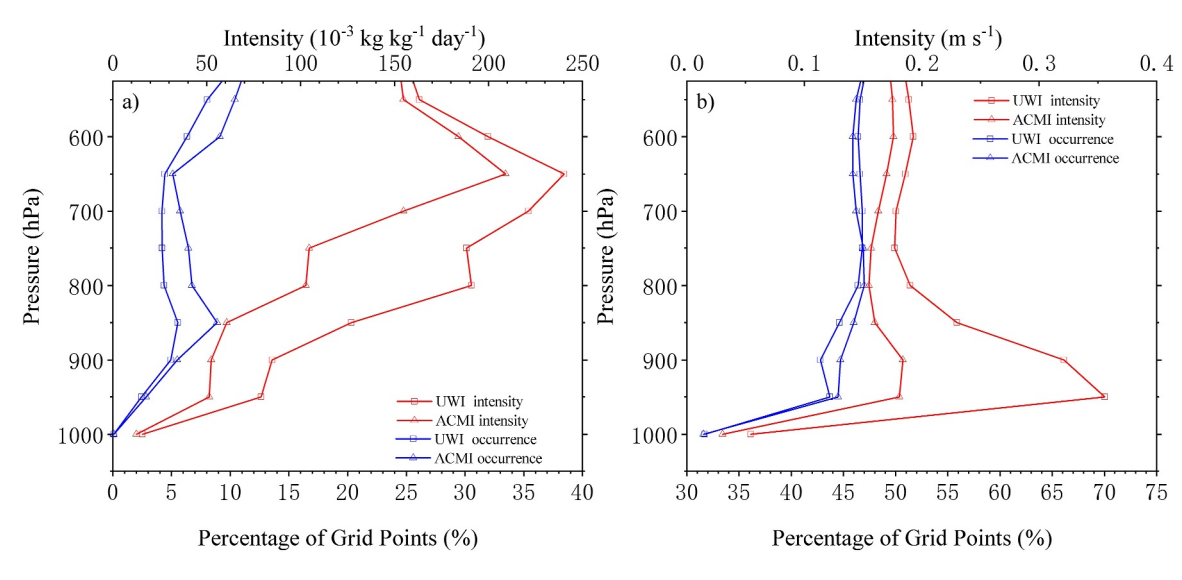
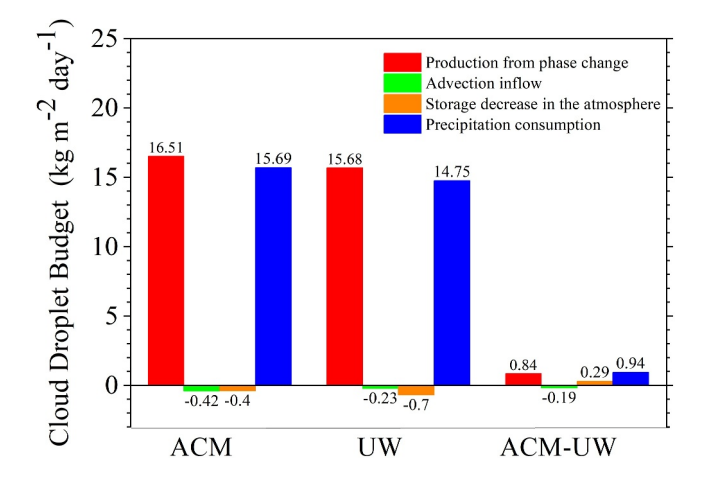


Figure 14. Percentage area (blue) and intensity (red) of (a) condensation  $(10^{-3} \text{ kg kg}^{-1} \text{ day}^{-1})$  and (b) ascending motion (m s<sup>-1</sup>) from the forecasts in the fine grid [I] planetary boundary layer (PBL) parameterization averaged in 11–16LT, comparing PBL schemes UW and ACM.

directly affecting the daytime precipitation intensity parameterized by the KF closure in [O]. When nested with [O] using a lower CUP frequency (CT30), selecting a different PBL scheme ACM, compared to MYJ, reduces over-forecasting in the early afternoon but intensifies it in the first-day morning and the first half of the second-day night (Figure S2 in Supporting Information S1). Thus, changing the PBL scheme alone has limited improvement on the forecast of diurnal precipitation variation in [I]. Conversely, when coupled with a high CUP frequency (CT1.5) in [O], using the same PBL scheme ACM significantly reduces the over-forecast in the first-day daytime (10–17LT) and evening (19–21LT) compared to MYJ.

Therefore, the PBL and cumulus parameterizations in the coarse grid [O] respectively control the generation of CAPE that supports convection and the consumption of CAPE through convective precipitation, which, in turn, determines the moisture convergence into the fine grid [I]. The same PBL parameterization in [I] transports surface heat and moisture fluxes into the lower troposphere. Different PBL schemes simulate varying depths, peak altitudes, and intensities of the heating and moistening layers due to differences in turbulent mixing. When the PBL and cumulus parameterizations are coupled coherently, they can jointly organize the mesoscale circulation, maintaining an appropriate balance of convective energy and water vapor supply that significantly improves forecasting the diurnal variation of precipitation in [I]. Isolating or dis-

jointly implementing these parameterizations between the nested grids may discount such improvements.



**Figure 15.** Cloud droplet budget (kg m<sup>-2</sup> day<sup>-1</sup>) and difference in the fine grid [I] planetary boundary layer (PBL) parameterization averaged in 11–16LT, comparing PBL schemes UW and ACM.

## 7. Summary and Conclusions

This study aims to determine and understand the effects of coupling cumulus and PBL parameterizations on forecasting diurnal precipitation variation through the double grid nesting approach. It is demonstrated by reinitialized 36-hr forecasts during the plum rainy season, 19 June–20 July 2016, in Jiangsu Province in China. The main findings are summarized below.

- 1. In the outer domain at 15 km grid [O], the control run coupling the MYJ PBL scheme with the KF cumulus scheme called at a time interval of 30 min (CT30) predicts the two precipitation peaks in early morning and early afternoon as observed, but significantly overestimates their intensities. While the afternoon peak is twice higher, both the evening valley and early morning peak are also significantly overpredicted.
- 2. In [O], the PBL and cumulus parameterizations affect respectively the accumulation and consumption of instability energy, jointly governing

MEI ET AL. 14 of 18

subgrid convective precipitation. Increasing the KF call frequency allows timely triggering and full development of convective activities during the daytime. Consequently, subgrid convective rainfall increases while grid-scale resolved precipitation decreases, alleviating the delay of the daytime cycle and thus reducing the over-forecast of the low valley and early-morning precipitation. Further coupling a proper PBL scheme that allows turbulent mixing to penetrate into a thicker layer reduces the CAPE accumulation and hence weakens the overprediction of the daytime precipitation and afternoon peaks. In particular, the ACM PBL scheme coupled with KF scheme at a high-frequency (CT1.5) predicts the thickest moistening layer and the weakest CAPE and consequently the most realistic precipitation diurnal variation in the coarse grid [O].

3. In the inner domain at 1 km grid [I], precipitation is explicitly resolved by cloud microphysics processes as driven by lateral boundary conditions from the coarse grid [O] coupling the PBL and cumulus parameterizations. The same PBL parameterization in [I] transports surface heat and moisture fluxes into the lower troposphere and contributes to precipitation formation. Increasing the KF frequency in [O] reduces the water vapor excess remaining in the low troposphere and thus provides less water vapor supply across the boundaries to weaken daytime [I] precipitation over-forecast. Meanwhile, different PBL schemes produce different vertical turbulent mixing with varying depths, peak altitudes, and intensities of the heating and moistening layers and consequently affect the CAPE accumulation rate and drive the convection and precipitation explicitly resolved as a coupled system by cloud microphysics processes in [I]. When the PBL and cumulus parameterizations are coupled coherently, the mesoscale circulation can be jointly represented alongside the appropriate balance of convective energy and moisture convergence. As a result, the precipitation diurnal cycle forecast in [I] could be greatly improved. In particular, the UW PBL scheme, when coupled with KF cumulus scheme at CT1.5, most realistically predicts the daytime precipitation peak.

Optimizing the KF frequency in [O] alone may lead to substantial over-forecast of the afternoon peak for both coarse and fine grids, while coupling a proper PBL scheme with a low KF frequency may worse the over-prediction of the evening valley in [O] and the morning and nighttime precipitation in [I]. Liang et al. (2019) argued that the convective instability or CAPE once generated in [O] needs to be consumed in certain rhythm, otherwise, it would be transported to release at unrealistic places and times, causing wrong rainfall spatiotemporal distribution. Our result above supports their argument. Therefore, in the double nesting approach, a coherent coupling between the cumulus and PBL parameterizations is essential to capture accurately the mesoscale circulation that drives consistent convective energy and water supply to determine correctly the diurnal precipitation variation in different stages.

In conclusion, the coherent coupling between the cumulus and PBL parameterizations significantly improves the forecast of Jiangsu precipitation diurnal cycle and daily variation. However, there is large room for further improvements. For example, the afternoon peak in [O] is still about 60% higher than observations. Refinements in CUP such as trigger functions and closure assumptions may help reduce overestimation (Sun & Liang, 2023). In addition, the precipitation peak time in the early morning for the second day forecast is generally 2–5 hr earlier than observations in both the coarse and fine grids. The early morning peak time during the plum rainy season typically lags the moisture convergence by about 3–4 hr (Xue et al., 2018), where large-scale circulation forcing errors are a major source of systematic biases (Guo et al., 2019). While some attempts have been made to attenuate these forcing errors through spectral nudging methods (Tang et al., 2010; Yang et al., 2019), a more robust approach is to incorporate accurate lateral boundary conditions across the [O] buffer zones (Liang et al., 2001) from directly improved global forecasts over the NCEP GFS used in this study.

## **Data Availability Statement**

The WRF V3.9.1 model could be downloaded at <a href="https://www2.mmm.ucar.edu/wrf/users/download/get\_sources.">html (Skamarock et al., 2008)</a>. The European Center for Medium-Range Weather Forecasts reanalysis (ERA5) data could be downloaded at <a href="https://www.ecmwf.int/en/forecasts/dataset/ecmwf-reanalysis-v5">https://www.ecmwf.int/en/forecasts/dataset/ecmwf-reanalysis-v5</a> (Hersbach et al., 2020). The observational data and model simulations used in this study are available from <a href="https://pan.baidu.com/s/1YAogl58hZ-rrhyFmpscEhQ">https://pan.baidu.com/s/1YAogl58hZ-rrhyFmpscEhQ</a>. They can be accessed but their usage may be restricted by pertinent Chinese government rules and regulations that are beyond the control of the authors.

MEI ET AL. 15 of 18

21698996



## Journal of Geophysical Research: Atmospheres

10.1029/2023JD040295

#### Acknowledgments

This work was primarily supported by the National Key R&D Program of China (2022YFC3003905, 2021YFC3000904), the Jiangsu Provincial Key Technology R&D Program (BE2022851), the Jiangsu Meteorological Bureau Key Research Fund Project (KZ202005), S&T Development Fund of Nanjing Joint Institute for Atmospheric Sciences (KJFZ202303), and the Basic Research Fund of Chinese Academy of Meteorological Sciences (2022Y019, 2021Y012). Additionally, Liang was supported by the U.S. National Science Foundation Innovations at the Nexus of Food, Energy and Water Systems under Grant EAR1903249.

#### References

- Bechtold, P., Semane, N., Lopez, P., Chaboureau, J.-P., Beljaars, A., & Bormann, N. (2014). Representing equilibrium and nonequilibrium convection in large-scale models. *Journal of the Atmospheric Sciences*, 71(2), 734–753. https://doi.org/10.1175/JAS-D-13-0163.1
- Bretherton, C. S., & Park, S. (2009). A New moist turbulence parameterization in the community atmosphere model. *Journal of Climate*, 22(12), 3422–3448. https://doi.org/10.1175/2008JCLI2556.1
- Cai, X., Shou, S., & Zhong, Q. (2006). Impact of different boundary layer parameterization schemes on the numerical simulation for a Rain Storm. Transactions of Atmospheric Sciences, 29(003), 364–370. (in Chinese). https://doi.org/10.3969/j.issn.1674-7097.2006.03.012
- Chou, M.-D., & Suarez, M. J. (1999). Technical report series on global modeling and data assimilation. In A solar radiation parameterization for atmospheric studies (Vol. 15, pp. 1–38). Goddard Space Flight Center.
- Correia, J., Arritt, R. W., & Anderson, C. J. (2008). Idealized mesoscale convective system structure and propagation using convective parameterization. *Monthly Weather Review*, 136(7), 2422–2442. https://doi.org/10.1175/2007MWR2229.1
- Del Genio, A. D., & Wu, J. (2010). The role of entrainment in the diurnal cycle of continental convection. *Journal of Climate*, 23(10), 2722–2738. https://doi.org/10.1175/2009JCLI3340.1
- Ding, Y. (1992). Summer monsoon rainfalls in China. Journal of the Meteorological Society of Japan, 70(1B), 373–396. https://doi.org/10.2151/imsi1965.70.1B 373
- Fritsch, J. M., & Kain, J. S. (1993). Convective parameterization for mesoscale models: The Fritsch-Chappell scheme. In: K. A. Emanuel & D. J. Raymond (Eds.), *The representation of cumulus convection in numerical models, Meteorological Monographs* (Vol. 24, pp. 159–164). American Meteorological Society. https://doi.org/10.1007/978-1-935704-13-3\_15
- Goines, D. C., & Kennedy, A. D. (2018). Precipitation from a multiyear database of convection-allowing WRF simulations. *Journal of Geophysical Research: Atmospheres*, 123(5), 2424–2453. https://doi.org/10.1002/2016JD026068
- Grell, G. A., & Freitas, S. R. (2014). A scale and aerosol aware stochastic convective parameterization for weather and air quality modeling. Atmosphere Chemistry and Physics, 14(10), 5233–5250. https://doi.org/10.5194/acp-14-5233-2014
- Guo, Z., Fang, J., Sun, X., Yang, Y., & Tang, J. (2019). Sensitivity of summer precipitation simulation to microphysics parameterization over eastern China: Convection-permitting regional climate simulation. *Journal of Geophysical Research: Atmospheres*, 124(16), 9183–9204. https://doi.org/10.1029/2019JD030295
- Gustafson, W. I., Jr., Ma, P.-L., & Singh, B. (2014). Precipitation characteristics of CAM5 physics at mesoscale resolution during MC3E and the impact of convective timescale choice. *Journal of Advances in Modeling Earth Systems*, 6(4), 1271–1287. https://doi.org/10.1002/2014MS000334
- He, J., Shen, X., Zhang, X., Zhou, W., & Feng, T. (2017). Analysis of dynamic structure in boundary layer during a torrential rainfall process on Meiyu front. *Journal of PLA University of Science and Technology(Natural Science Edition)*, 1–7. (in Chinese). https://doi.org/10.12018/j.issn. 1009-3443.20170211001
- He, X., Kim, H., Kirstetter, P.-E., Yoshimura, K., Chang, E.-C., Ferguson, C. R., et al. (2015). The diurnal cycle of precipitation in regional spectral model simulations over West Africa: Sensitivities to resolution and cumulus schemes. *Weather and Forecasting*, 30(2), 424–445. https://doi.org/10.1175/WAF-D-14-00013.1
- Hersbach, H., Bell, B., Berrisford, P., Hirahara, S., Horányi, A., Muñoz-Sabater, J., et al. (2020). The ERA5 global reanalysis. *Quarterly Journal of the Royal Meteorological Society*, 146(730), 1999–2049. https://doi.org/10.1002/qj.3803
- Hong, S.-Y., Noh, Y., & Dudhia, J. (2006). A new vertical diffusion package with an explicit treatment of entrainment processes. *Monthly Weather Review*, 134(9), 2318–2341. https://doi.org/10.1175/MWR3199.1
- Janjić, Z. I. (1994). The step-mountain eta coordinate model: Further developments of the convection, viscous sublayer, and turbulence closure schemes. Monthly Weather Review, 122(5), 927–945. https://doi.org/10.1175/1520-0493(1994)122<0927:TSMECM>2.0.CO;2
- Janjić, Z. I. (1996). The surface layer in the NCEP Eta model, paper presented at eleventh conference on numerical weather prediction. American Meteorological Society.
- Jiao, D., Xu, N., Yang, F., & Xu, K. (2021). Evaluation of spatial-temporal variation performance of ERA5 precipitation data in China. Scientific Reports, 11(1), 17956. https://doi.org/10.1038/s41598-021-97432-y
- Jiménez, P. A., Dudhia, J., González-Rouco, J. F., Navarro, J., Montávez, J. P., & García-Bustamante, E. (2012). A revised scheme for the WRF surface layer formulation. *Monthly Weather Review*, 140(3), 898–918. https://doi.org/10.1175/MWR-D-11-00056.1
- Jin, E. K., Choi, I.-J., Kim, S.-Y., & Han, J.-Y. (2016). Impact of model resolution on the simulation of diurnal variations of precipitation over East Asia. Journal of Geophysical Research: Atmospheres, 121(4), 1652–1670. https://doi.org/10.1002/2015JD023948
- Kain, J. S. (2004). The Kain–Fritsch convective parameterization: An update. Journal of Applied Meteorology, 43(1), 170–181. https://doi.org/10.1175/1520-0450(2004)043<0170:TKCPAU>2.0.CO:2
- Konduru, R. T., & Takahashi, H. G. (2020). Effects of convection representation and model resolution on diurnal precipitation cycle over the Indian monsoon region: Toward a convection-permitting regional climate simulation. *Journal of Geophysical Research: Atmospheres*, 125(16), e2019JD032150. https://doi.org/10.1029/2019JD032150
- Koo, M.-S., & Hong, S.-Y. (2010). Diurnal variations of simulated precipitation over East Asia in two regional climate models. *Journal of Geophysical Research*, 115(D5), 458–473. https://doi.org/10.1029/2009JD012574
- Liang, X.-Z., Kunkel, K. E., & Samel, A. N. (2001). Development of a regional climate model for U.S. Midwest applications. Part I: Sensitivity to buffer zone treatment. *Journal of Climate*, 14(23), 4363–4378. https://doi.org/10.1175/1520-0442(2001)014<4363:DOARCM>2.0.CO;2
- Liang, X.-Z., Li, L., Dai, A., & Kunkel, K. E. (2004). Regional climate model simulation of summer precipitation diurnal cycle over the United States. Geophysical Research Letters, 31(24). https://doi.org/10.1029/2004GL021054
- Liang, X.-Z., Li, Q., Mei, H., & Zeng, M. (2019). Multi-grid nesting ability to represent convections across the gray zone. Journal of Advances in Modeling Earth Systems, 11(12), 4352–4376. https://doi.org/10.1029/2019MS001741
- Mlawer, E. J., Taubman, S. J., Brown, P. D., Iacono, M. J., & Clough, S. A. J. J. o. G. R. A. (1997). Radiative transfer for inhomogeneous atmospheres: RRTM, a validated correlated-k model for the longwave. *Journal of Geophysical Research*, 102(D14), 16663–16682. https://doi.org/10.1029/97JD00237
- Mooney, P. A., Broderick, C., Bruyère, C. L., Mulligan, F. J., & Prein, A. F. (2017). Clustering of observed diurnal cycles of precipitation over the United States for evaluation of a WRF multiphysics regional climate ensemble. *Journal of Climate*, 30(22), 9267–9286. https://doi.org/10.1175/JCL-D-16-0851
- Pei, L., Moore, N., Zhong, S., Luo, L., Hyndman, D. W., Heilman, W. E., & Gao, Z. (2014). WRF model sensitivity to land surface model and cumulus parameterization under short-term climate extremes over the Southern Great Plains of the United States. *Journal of Climate*, 27(20), 7703–7724. https://doi.org/10.1175/JCLI-D-14-00015.1

MEI ET AL. 16 of 18

21698996



## Journal of Geophysical Research: Atmospheres

- 10.1029/2023JD040295
- Pleim, J. E. (2007). A combined local and nonlocal closure model for the atmospheric boundary layer. Part I: Model description and testing. *Journal of Applied Meteorology and Climatology*, 46(9), 1383–1395. https://doi.org/10.1175/JAM2539.1
- Qiao, F., & Liang, X.-Z. (2015). Effects of cumulus parameterizations on predictions of summer flood in the Central United States. *Climate Dynamics*, 45(3), 727–744. https://doi.org/10.1007/s00382-014-2301-7
- Qiao, F., & Liang, X.-Z. (2016). Effects of cumulus parameterization closures on simulations of summer precipitation over the United States coastal Oceans. *Journal of Advances in Modeling Earth Systems*, 8(2), 764–785. https://doi.org/10.1002/2015MS000621
- Samel, A. N., Wang, W., & Liang, X. (1999). The monsoon rainband over China and relationships with the Eurasian circulation. *Journal of Climate*, 12(1), 115–131. https://doi.org/10.1175/1520-0442(1999)012<0115:TMROCA>2.0.CO;2
- Schwartz, C. S., Kain, J. S., Weiss, S. J., Xue, M., Bright, D. R., Kong, F., et al. (2010). Toward improved convection-allowing ensembles: Model physics sensitivities and optimizing probabilistic guidance with small ensemble membership. Weather and Forecasting, 25(1), 263–280. https://doi.org/10.1175/2009waf2222267.1
- Shen, X., Ma, Z., Guo, C., & Li, X. (2017). The effect of boundary layer parameterization schemes on the simulation of turbulent exchange properites of a Mei-Yu rainstorm. *Journal of Tropical Meteorology*, 033(006), 793–811. (in Chinese). https://doi.org/10.16032/j.issn.1004-4965.2017.06.001
- Skamarock, W. C., Klemp, J. B., Dudhia, J., Gill, D. O., Barker, D. M., Duda, M. G., et al. (2008). A description of the advanced research WRF version 3. In NCAR technical note, NCAR/TN-475+STR (p. 125). National Center for Atmospheric Research. https://doi.org/10.5065/D68S4MVH
- Sun, C., & Liang, X.-Z. (2023). Understanding and reducing warm and dry summer biases in the central United States: Improving cumulus parameterization. *Journal of Climate*, 136(7), 2035–2054. https://doi.org/10.1175/JCLI-D-22-0254.1
- Tan, C., Liu, Q., & Ma, Z. (2013). Influences of sub-grid convective processes on cloud forecast in the GRAPES global model. Acta Meteorologica Sinica, 71(5), 867–878. (in Chinese). https://doi.org/10.11676/qxxb2013.067
- Tang, J., Song, S., & Wu, J. (2010). Impacts of the spectral nudging technique on simulation of the East Asian summer monsoon. *Theoretical and Applied Climatology*, 101(1–2), 41–51. https://doi.org/10.1007/s00704-009-0202-1
- Tang, S., Gleckler, P., Xie, S., Lee, J., Ahn, M. S., Covey, C., & Zhang, C. (2021). Evaluating the diurnal and semidiurnal cycle of precipitation in CMIP6 models using satellite-and ground-based observations. *Journal of Climate*, 34(8), 3189–3210. https://doi.org/10.1175/JCLI-D-20-0639.1
- Tao, S., & Chen, L. (1987). A review of recent research on the East Asian summer monsoon in China. In C.-P. Chang & T. N. Krishnamurti (Eds.), Monsoon meteorology (pp. 60–92). Oxford University Press.
- Tewari, M., Chen, F., Wang, W., Dudhia, J., Lemone, M. A., Mitchell, K. E., et al. (2004). Implementation and verification of the unified NOAH land-surface model in the WRF model. *In Paper presented at 20th conference on weather analysis and forecasting/16th conference on numerical weather prediction* (Vol. 1115, pp. 11–15). American Meteorological Society.
- Thompson, G., Field, P. R., Rasmussen, R. M., & Hall, W. D. (2008). Explicit forecasts of winter precipitation using an improved bulk microphysics scheme. Part II: Implementation of a new snow parameterization. *Monthly Weather Review*, 136(12), 5095–5115. https://doi.org/10.1175/2008mwr2387.1
- Wang, D., Xu, G., & Jia, L. (2013). The evaluation of cumulus parameterization schemes in GRAPES model and its improved experiments. Meteorological Monthly, 39(2), 166–179. (in Chinese). https://doi.org/10.7519/j.issn.1000-0526.2013.02.005
- Wang, R., Zhu, Y., Qiao, F., Liang, X.-Z., Zhang, H., & Ding, Y. (2021). High-resolution simulation of an extreme heavy rainfall event in Shanghai using WRF: Sensitivity to planetary boundary layer parameterization. Advances in Atmospheric Sciences, 38(1), 98–115. https://doi. org/10.1007/s00376-020-9255-y
- Wang, Y., Zhou, L., & Hamilton, K. (2007). Effect of convective entrainment/detrainment on the simulation of the tropical precipitation diurnal cycle. *Monthly Weather Review*, 135(2), 567–585. https://doi.org/10.1175/MWR3308.1
- Warner, T. T., & Hsu, H.-M. (2000). Nested-model simulation of moist convection: The impact of coarse-grid parameterized convection on fine-grid resolved convection. *Monthly Weather Review*, 128(7), 2211–2231. https://doi.org/10.1175/1520-0493(2000)128<2211:NMSOMC>2.0.
- Wong, M., Romine, G., & Snyder, C. (2020). Model improvement via systematic investigation of physics tendencies. *Monthly Weather Review*, 148(2), 671–688. https://doi.org/10.1175/MWR-D-19-0255.1
- Xu, H., Zhu, Y., Liu, R., Shen, H., Wang, D., & Zhai, G. (2013). Eulation experiments with different planetary boundary layer schemes in the lower reaches of the Yangtze River. *Chinese Journal of Atmospheric Sciences*, 37(1), 149–159. (in Chinese). https://doi.org/10.3878/j.issn. 1006-9895.2012.12021
- Xu, W., & Zipser, E. J. (2011). Diurnal variations of precipitation, deep convection, and lightning over and east of the eastern Tibetan Plateau. Journal of Climate, 24(2), 448–465. https://doi.org/10.1175/2010JCLI3719.1
- Xue, M., Luo, X., Zhu, K., Sun, Z., & Fei, J. (2018). The controlling role of boundary layer inertial oscillations in Mei-Yu frontal precipitation and its diurnal cycles over China. *Journal of Geophysical Research: Atmospheres*, 123(10), 5090–5115. https://doi.org/10.1029/2018JD028368
- Yang, B., Zhou, Y., Zhang, Y., Huang, A., Qian, Y., & Zhang, L. (2018). Simulated precipitation diurnal cycles over East Asia using different CAPE-based convective closure schemes in WRF model. Climate Dynamics, 50(5), 1639–1658. https://doi.org/10.1007/s00382-017-3712-z
- Yang, L., Wang, S., Tang, J., Niu, X., & Fu, C. (2019). Impact of nudging parameters on dynamical downscaling over CORDEX East Asia phase II domain: The case of summer 2003. *Journal of Applied Meteorology and Climatology*, 58(12), 2755–2771. https://doi.org/10.1175/Jamc-D-19.0152.1
- Yu, R., Zhou, T., Xiong, A., Zhu, Y., & Li, J. (2007). Diurnal variations of summer precipitation over contiguous China. Geophysical Research Letters, 34(1). https://doi.org/10.1029/2006GL028129
- Yuan, W., Yu, R., Zhang, M., Lin, W., Li, J., & Fu, Y. (2013). Diurnal cycle of summer precipitation over subtropical East Asia in CAM5. *Journal of Climate*, 26(10), 3159–3172. https://doi.org/10.1175/JCLI-D-12-00119.1
- Zhang, G., Cook, K. H., & Vizy, E. K. (2016). The diurnal cycle of warm season rainfall over West Africa. Part II: Convection-permitting simulations. *Journal of Climate*, 29(23), 8439–8454. https://doi.org/10.1175/JCLI-D-15-0875.1
- Zhang, Y., & Chen, H. (2016). Comparing CAM5 and superparameterized CAM5 simulations of summer precipitation characteristics over continental East Asia: Mean state, frequency-intensity relationship, diurnal cycle, and influencing factors. *Journal of Climate*, 29(3), 1067–1089. https://doi.org/10.1175/JCLI-D-15-0342.1
- Zheng, Y., Alapaty, K., Herwehe, J. A., Del Genio, A. D., & Niyogi, D. (2016). Improving high-resolution weather forecasts using the Weather Research and Forecasting (WRF) model with an updated Kain–Fritsch scheme. *Monthly Weather Review*, 144(3), 833–860. https://doi.org/10. 1175/MWR-D-15-0005.1

MEI ET AL. 17 of 18



## Journal of Geophysical Research: Atmospheres

10.1029/2023JD040295

Zhou, Z., Chen, S., Li, Z., & Luo, Y. (2023). An evaluation of CRA40 and ERA5 precipitation products over China. *Remote Sensing*, 15(22), 5300. https://doi.org/10.3390/rs15225300

Zhu, K., Xue, M., Zhou, B., Zhao, K., Sun, Z., Fu, P., et al. (2018). Evaluation of real-time convection-permitting precipitation forecasts in China during the 2013–2014 summer season. *Journal of Geophysical Research: Atmospheres*, 123(2), 1037–1064. https://doi.org/10.1002/2017JD027445

MEI ET AL. 18 of 18